Insight Into the Role of PC$_{71}$BM on Enhancing the Photovoltaic Performance of Ternary Organic Solar Cells

Bei Wang [1,2], Yingying Fu [1], Chi Yan [1,3], Rui Zhang [1,3], Qingqing Yang [1], Yanchun Han [1] and Zhiyuan Xie [1*]

[1] State Key Laboratory of Polymer Physics and Chemistry, Changchun Institute of Applied Chemistry, Chinese Academy of Sciences, Changchun, China, [2] University of Science and Technology of China, Hefei, China, [3] University of Chinese Academy of Sciences, Beijing, China

The development of non-fullerene acceptor molecules have remarkably boosted power conversion efficiency (PCE) of polymer solar cells (PSCs) due to the improved spectral coverage and reduced energy loss. An introduction of fullerene molecules into the non-fullerene acceptor-based blend may further improve the photovoltaic performance of the resultant ternary PSCs. However, the underlying mechanism is still debatable. Herein, the ternary PSCs based on PBDB-T:ITIC:PC$_{71}$BM blend were fabricated and its PCE was increased to 10.2% compared to 9.2% for the binary PBDB-T:ITIC devices and 8.1% for the PBDB-T:PC$_{71}$BM PSCs. Systematic investigation was carried out to disclose the effect of PC$_{71}$BM on the blend morphology and charge transport behavior. It is found that the PC$_{71}$BM tends to intermix with the PBDB-T donor compared to the ITIC counterpart. A small amount of PC$_{71}$BM in the ternary blend is helpful for ITIC to aggregate and form efficient electron-transport pathways. Accordingly, the electron mobility is increased and the density of electron traps is decreased in the ternary blend in comparison with the PBDB-T:ITIC blend. Finally, the suppressed bimolecular recombination and enhanced charge collection lead to high PCE for the ternary solar cells.

Keywords: ternary organic solar cells, morphology, aggregation, charge transport, trap density

INTRODUCTION

Non-fullerene acceptors have drawn great research interests in the community of polymer solar cells (PSCs) in recent years. The power conversion efficiencies (PCE) of PSCs employing non-fullerene acceptors have increased rapidly as compared to the PSCs using fullerene derivatives as acceptors (Lin et al., 2015; Cao et al., 2017; Fan et al., 2017; Li et al., 2017; Xiao et al., 2017; Dai et al., 2018). Non-fullerene acceptors possess some advantages such as strong absorption in the visible region and tunable energy levels with regard to fullerene derivatives, and thus allows for suitable combination of donor/acceptor blend to improve the spectral coverage and reduce the energy loss (Holliday et al., 2016; Li et al., 2016, 2018; Qiu et al., 2017). In addition to the strong and complementary absorption and the matched energy levels of the donor/acceptor combination, the donor/acceptor morphology with a suitable phase separation is equally important for realizing a high PCE. More recently, addition of another type of donor or acceptor in the binary non-fullerene PSCs to fabricate so-called ternary PSCs have drawn great interests. This kind of ternary strategy

is to some extent powerful to enhance the photovoltaic performance of the devices (Cheng et al., 2014; Gasparini et al., 2016). As it is argued, ternary PSCs possess some features such as more complementary absorption (Jiang et al., 2018) and more appropriate microstructure relative to the binary counterparts (Wang et al., 2017) and easier fabrication compared with tandem solar cells. With these superiorities, ternary PSCs have developed very quickly and become a research focus in the field (Yu et al., 2017; Zhang G. et al., 2017; Zhao et al., 2017; Wang et al., 2018). Nonetheless, the morphology of ternary blends is more complex resulting in the underlying mechanism debatable. It is proposed that the ternary morphology can be divided into four types according to the relative position of third component to the donor phases and acceptor phases, namely the third component embedded in one phase, located at the interfaces, formed alloy structure with either the donor or acceptor material and parallel-like bulk heterojunction structure with the donor or acceptor (Lu et al., 2015). In fact, the ternary morphology is too complicated to be clearly identified using the current technology. Typical electron acceptor fullerene derivatives, such as $PC_{71}BM$ and Bis-$PC_{71}BM$ have been used as additives in non-fullerene PSCs. For example, Bo et al. have reported high-performance ternary PSCs employing non-fullerene and fullerene acceptors simultaneously for the first time, in which they found that a small amount of fullerene is in favor of boosting the photovoltaic performance of the devices (Lu et al., 2016). Hou et al. also reported the high-efficiency ternary PSCs using Bis-$PC_{71}BM$ as the third component (Zhao et al., 2017). They proposed that Bis-$PC_{71}BM$ mainly exists in the upper surface of active layer and promotes electron transport in their ternary blend PSCs.

For the ternary PSCs, the third component such as $PC_{71}BM$ may have strong effect on the resultant ternary morphology and hence its photovoltaic properties. Although some researches on the function of third component were carried out (Yu et al., 2017; Zhang J. et al., 2017; Wang et al., 2018), the underlying mechanism is still debatable.

Herein, a reported wide bandgap polymer poly[(2,6-(4,8-bis(5-(2-ethylhexyl)thiophen-2-yl)-benzo[1,2-b:4,5-b′] dithiophene))-alt-(5,5-(1′,3′-di-2-thienyl-5′,7′-bis(2-ethylhexyl) benzo[1′,2′-c:4′,5′-c′]dithiophene-4,8-dione))] (PBDB-T) is used as the donor, organic molecule (3,9-bis(2-methylene-(3-(1,1-dicyanomethylene)-indanone))-   5,5,11,11-tetrakis(4-hexylphenyl)-dithieno[2,3-d:2′,3′-d′]-s-indaceno[1,2-b:5,6-b′] dithiophene) (ITIC) is used as the acceptor and [6,6]-phenyl-C71-butyric acid methyl ester ($PC_{71}BM$) is used as the third component to prepare the ternary PSCs. The optimized PSCs based on ternary PBDB-T:ITIC:$PC_{71}BM$ blend demonstrate a higher PCE of 10.2% than 9.2% of the binary PBDB-T:ITIC devices and 8.1% of the PBDB-T:$PC_{71}BM$ PSCs. Further studies are mainly focused on the effect of $PC_{71}BM$ on the blend morphology and charge transport behavior. It is found that the $PC_{71}BM$ tends to intermix with the PBDB-T donor compared to the ITIC counterpart. A small amount of $PC_{71}BM$ in the ternary blend is helpful for ITIC to aggregate and form efficient electron-transport pathways. Accordingly, the electron mobility is increased and the density of electron traps is decreased in the ternary blend in comparison with the PBDB-T:ITIC blend. Finally, the suppressed bimolecular recombination and enhanced charge collection lead to an enhanced PCE for the ternary solar cells.
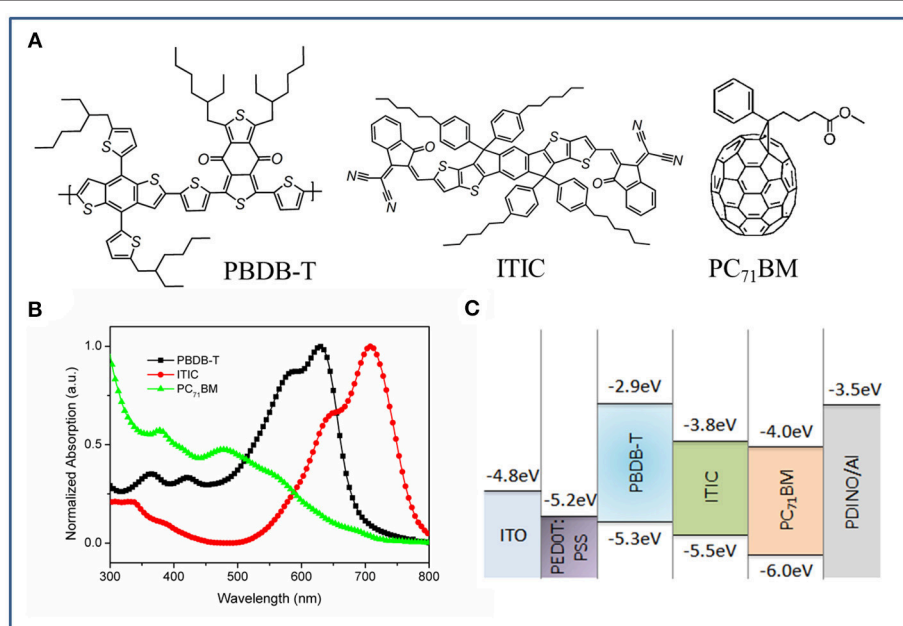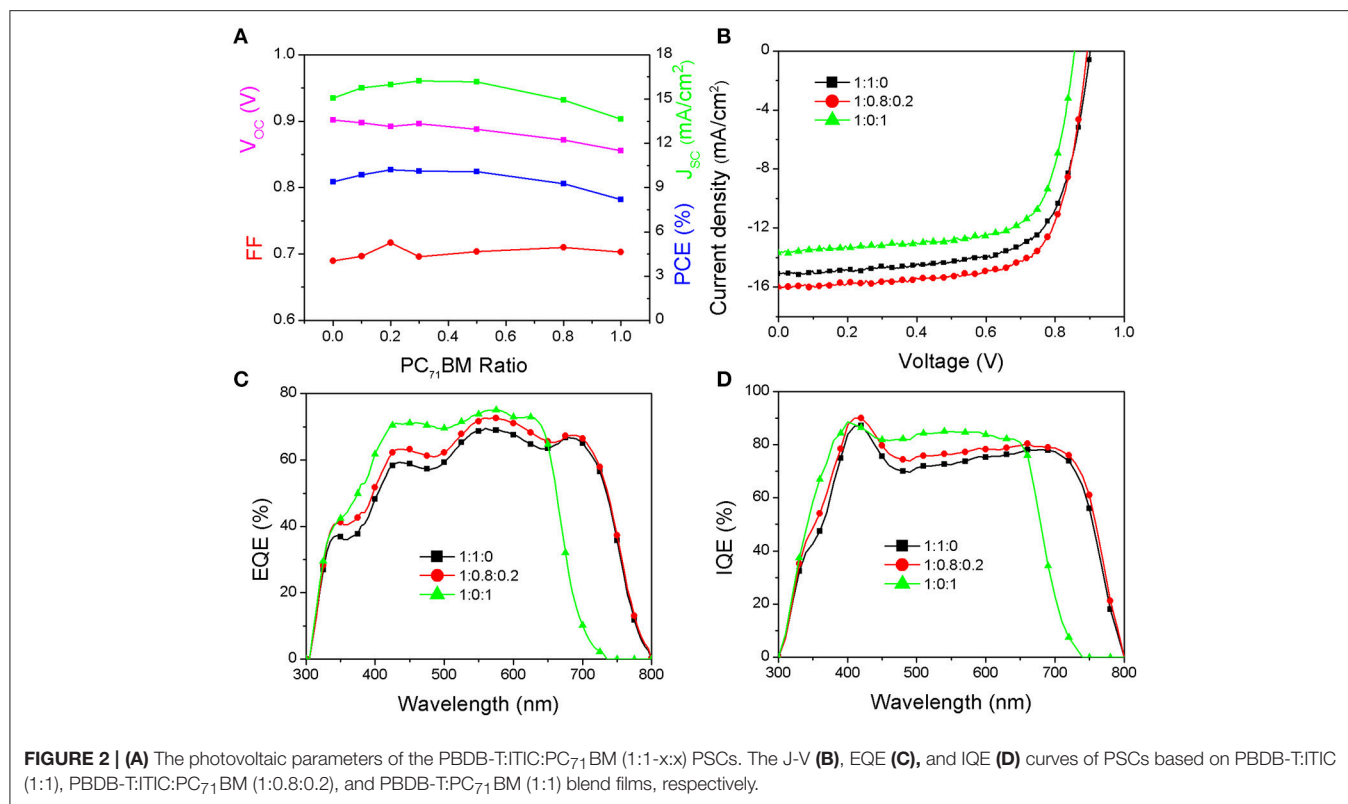

FIGURE 1 | (A) Chemical structures of PBDB-T, ITIC, and $PC_{71}BM$. **(B)** Normalized absorption of pure PBDB-T, ITIC, and $PC_{71}BM$ films. **(C)** Energy level diagram of solar cells.

FIGURE 2 | (A) The photovoltaic parameters of the PBDB-T:ITIC:PC$_{71}$BM (1:1-x:x) PSCs. The J-V **(B)**, EQE **(C)**, and IQE **(D)** curves of PSCs based on PBDB-T:ITIC (1:1), PBDB-T:ITIC:PC$_{71}$BM (1:0.8:0.2), and PBDB-T:PC$_{71}$BM (1:1) blend films, respectively.

EXPERIMENTAL SECTION

Both the polymer PBDB-T donor and small molecule ITIC acceptor were bought from Solarmer Ltd. The PBDB-T has a molecular weight Mn of 21.5 kDa and a PDI of 1.9. PC$_{71}$BM was bought from American Dye Source. The interfacial material PDINO was provided by Dr. Zhiguo Zhang in Institute of Chemistry, Chinese Academy of Sciences. All materials were used as received without further purification.

Polymer solar cells were fabricated with a structure of ITO/PEDOT: PSS/active layer/PDINO/Al. The ITO substrates were subject to routine cleaning procedure of detergent, acetone and deionized water. After drying in an oven for 30 min, the ITO substrates were treated with UV-ozone for 25 min. The PEDOT:PSS layer was first deposited via spin-coating and dried at 140°C for 30 min in air. The subsequent active layer and buffer layer were spin-coated in a glove box. The active layers consisting of PBDB-T:PC$_{71}$BM, PBDB-T:ITIC, or ternary PBDB-T:ITIC:PC$_{71}$BM were spin-coated from their respective solutions in CB containing 0.5% DIO with a total concentration of 20 mg/mL. The spin-coating rate for the active layers was kept at 2,500 rpm for 1 min. The samples were annealed at 160°C for 10 min. A cathode buffer layer of PDINO was spin-coated on the active layer from its methanol solution with a concentration of 1 mg/mL at 3,000 rpm for 30 s. Finally, the Al cathode with a thickness of 100 nm was thermally deposited in a vacuum chamber. The electron—and hole-only devices were fabricated under the same procedure with a structure of ITO/PEIE/active

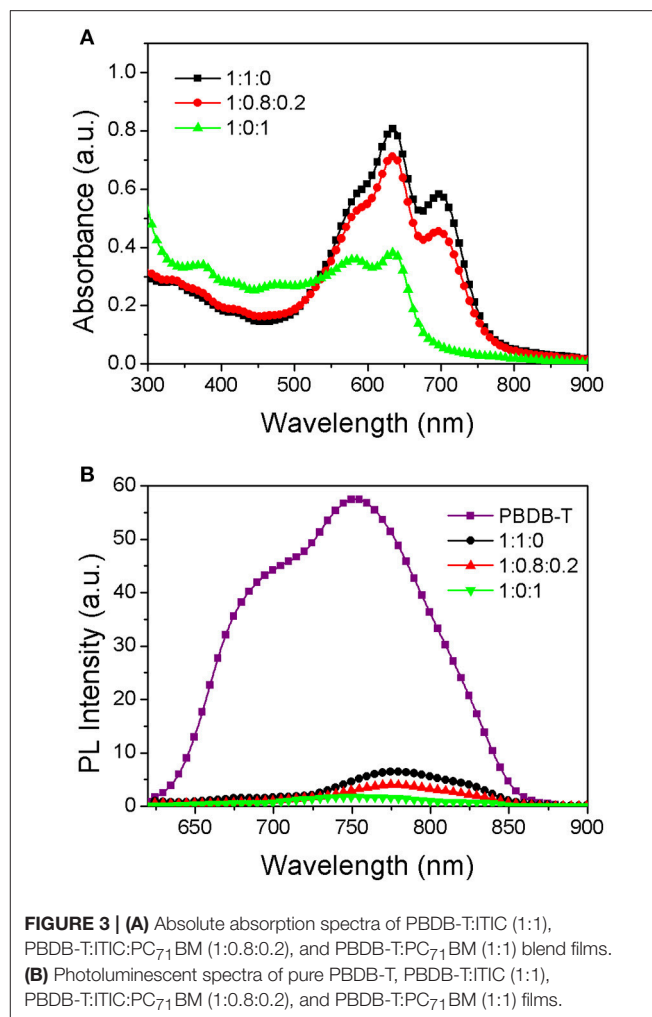layer/PDINO/Al and ITO/PEDOT:PSS/active layer/MoO$_3$/Al, respectively.

The current density-voltage (J-V) curves of the PSCs were traced by a computer-controlled Keithley 2400 Source Meter under simulated solar light illumination (AM 1.5G, 100 mW/cm^2). The EQE data were measured by solar cell spectral response measurement system (QE-R 3011, Enli Tech. Co.). The film absorption and fluorescence spectra were recorded on Agilent Cary 60UV-Vis spectrophotometer and Perkin-Elmer LS 55 spectrofluorometer, respectively. The thicknesses of individual layers were measured with a surface profilometer. The 2D-GIXD data were acquired at station 14B in Shanghai Synchrotron Radiation Facility.

RESULTS AND DISCUSSION

The chemical structures of PBDB-T, ITIC and PC$_{71}$BM are shown in **Figure 1A**. The normalized UV-vis absorption spectra of neat PBDB-T, ITIC and PC$_{71}$BM films are plotted in **Figure 1B**. It is clearly seen from **Figure 1B** that the main peaks of PBDB-T and ITIC are located at 625 and 710 nm, respectively, and their complementary absorption can strongly improve the spectral coverage in the visible region. PC$_{71}$BM exhibits absorption in short wavelength region but its absorption capability is relatively weak. In this study, the PSCs with a conventional device structure of ITO/PEDOT:PSS/active layer/PDINO/Al were fabricated, and their energy levels were plotted in **Figure 1C**. The polymer PDINO was used as cathode buffer layer referenced to the
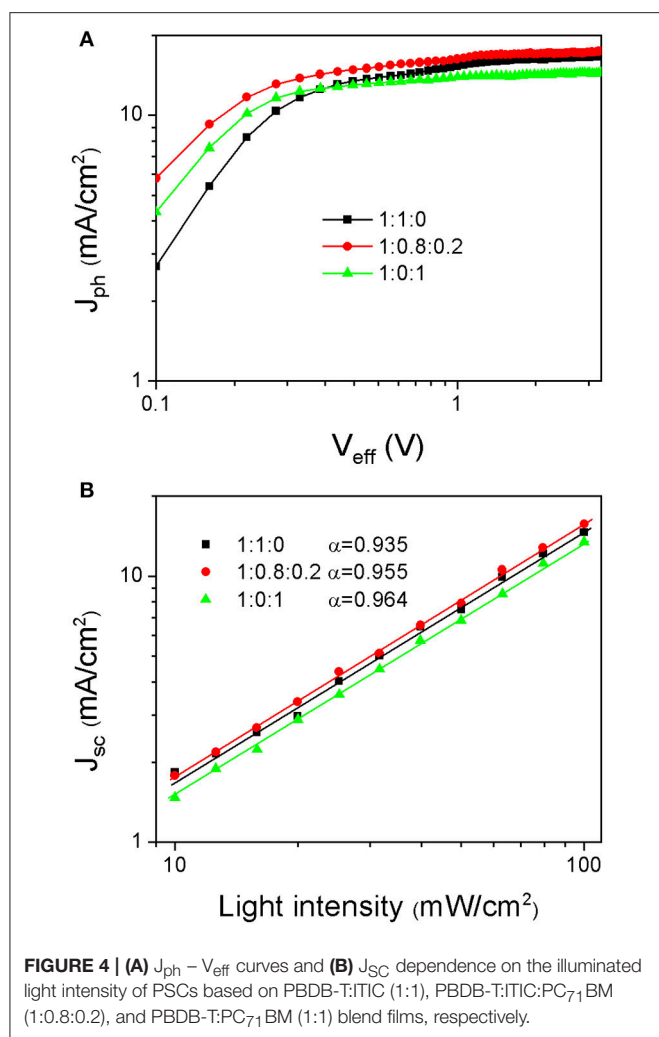
literature (Zhang Z. et al., 2014). The total ratio of donor component to acceptor component is kept at a fixed ratio of 1:1 (w/w). The ratio of PBDB-T:ITIC:PC$_{71}$BM is marked as the D:A1:A2.

The photovoltaic performance of the PSCs based on the PBDB-T:ITIC:PC$_{71}$BM (1:1-x:x) blend were firstly evaluated. The ratio of A1:A2 is varied from 1:0 to 0:1 while the ratio of D:(A1+A2) is fixed at 1:1 in order to keep a constant active layer thickness. The detailed photovoltaic parameters of the resultant PSCs with different ratio of two acceptors are listed in Table S1 in Supplementary Information. The dependence of V$_{OC}$, J$_{SC}$, FF, and PCE on the PC$_{71}$BM content for the resultant PSCs are plotted in **Figure 2A**. In the case of V$_{OC}$, it undergoes gradually decrease from 0.902 V for the binary PBDB-T:ITIC PSCs to 0.856 V for the binary PBDB-T: PC$_{71}$BM PSCs with increasing PC$_{71}$BM content from 0 to 1 in the ternary blend PSCs. The change is reasonable since the LUMO of ITIC is higher than that of PC$_{71}$BM, and the electron transport and collection will occur in PC$_{71}$BM phases when the PC$_{71}$BM amount is larger. The interesting thing is that the J$_{SC}$ are initially increased and then decreased with the increase of PC$_{71}$BM contents for the resultant ternary PSCs. The FF shows similar trend. Considering the intrinsic absorption properties between ITIC and PC$_{71}$BM, the substitution of small amount of ITIC by PC$_{71}$BM would decrease the total absorption of the ternary PBDB-T:ITIC:PC$_{71}$BM blend active layer. Thus, the improved J$_{SC}$ and FF for the ternary PBDB-T:ITIC:PC$_{71}$BM PSCs may imply that both the exciton dissociation and charge-collection efficiencies are enhanced in comparison to the binary PBDB-T:ITIC PSCs. It is plotted the illuminated J-V curves of the PBDB-T:ITIC PSCs, the PBDB-T:PC$_{71}$BM PSCs and the optimized ternary PBDB-T:ITIC:PC$_{71}$BM PSCs in **Figure 2B**, respectively. The non-fullerene PSCs based on binary PBDB-T:ITIC blend demonstrate a V$_{OC}$ of 0.902 V, a J$_{SC}$ of 15.06 mA/cm^2, a FF of 0.69, respectively, leading to a PCE of 9.38%. Due to the limited spectral coverage, the PBDB-T:PC$_{71}$BM PSCs show a lower J$_{SC}$ of 13.64 mA/cm^2, and finally result in a PCE of 8.21% together with a V$_{OC}$ of 0.856 V and a FF of 0.703. The ternary PBDB-T:ITIC:PC$_{71}$BM (1:0.8:0.2) PSCs demonstrate a V$_{OC}$ of 0.892 V, a J$_{SC}$ of 15.98 mA/cm^2, a FF of 0.717 and an overall PCE of 10.22%. Although the V$_{OC}$ is a little lowered in comparison to the binary PBDB-T:ITIC PSCs, the increased J$_{SC}$ and FF boost the PCE enhancement of the ternary PSCs. The external quantum efficiency (EQE) curves of the three devices are shown in **Figure 2C**. The spectral response of the PBDB-T:PC$_{71}$BM PSCs cover at a range of 300–700 nm with EQE higher than 70% at 450–650 nm. The PBDB-T:ITIC PSCs show extended spectral coverage of 300–800 nm due to the narrow bandgap of ITIC. The ternary PBDB-T:ITIC:PC$_{71}$BM PSCs show similar spectral response profile but high EQE compared to the PBDB-T:ITIC PSCs. The internal quantum efficiency (IQE) of these devices are also measured to clarify the absolute quantum efficiency in these devices and the curves are plotted in **Figure 2D**. It indicates that the photon-to-electron conversion efficiency is really improved by adding some amount of PC$_{71}$BM into the PBDB-T:ITIC blend. The absorption spectra of the active layers in three kinds of PSCs are plotted in **Figure 3A**.

FIGURE 3 | (A) Absolute absorption spectra of PBDB-T:ITIC (1:1), PBDB-T:ITIC:PC$_{71}$BM (1:0.8:0.2), and PBDB-T:PC$_{71}$BM (1:1) blend films. (B) Photoluminescent spectra of pure PBDB-T, PBDB-T:ITIC (1:1), PBDB-T:ITIC:PC$_{71}$BM (1:0.8:0.2), and PBDB-T:PC$_{71}$BM (1:1) films.

The PBDB-T:ITIC:PC$_{71}$BM (1:0.8:0.2) active layer shows a little low absorption at 550–750 nm due to decreased ITIC content compared to the PBDB-T:ITIC (1:1) film. Although the PBDB-T:PC$_{71}$BM (1:1) film demonstrates enhanced absorption at 300–500 nm, its absorption at 550–700 nm is remarkably decreased. Photoluminescence (PL) quenching experiments were carried out to check the charge transfer status in these films. As shown in **Figure 3B**, the introduction of PC$_{71}$BM favors to quench the excitons dominated on the PBDB-T donor.

The relationship between photocurrent (J$_{ph}$) and effective voltage (V$_{eff}$) is investigated to judge the charge generation and collection status in the PSCs based on the PBDB-T:ITIC (1:1), PBDB-T:ITIC:PC$_{71}$BM (1:0.8:0.2), and PBDB-T:PC$_{71}$BM (1:1) blends (Yuan et al., 2017; Zhang G. et al., 2017). As shown in **Figure 4A**, J$_{ph}$ is given by J$_{ph}$ = J$_L$ − J$_D$, where J$_L$ & J$_D$ are the current density under illumination and in the dark, respectively. V$_{eff}$ is defined as V$_0$ − V$_{appl}$, V$_0$ is the voltage when J$_{ph}$ = 0 and V$_{appl}$ is the applied voltage during the measurement. The J$_{ph}$ is supposed to be saturated at a V$_{eff}$ of 3 V, which are 16.55 mA/cm^2, 17.40 mA/cm^2 and 14.45 mA/cm^2, respectively, for the PSCs based on the PBDB-T:ITIC
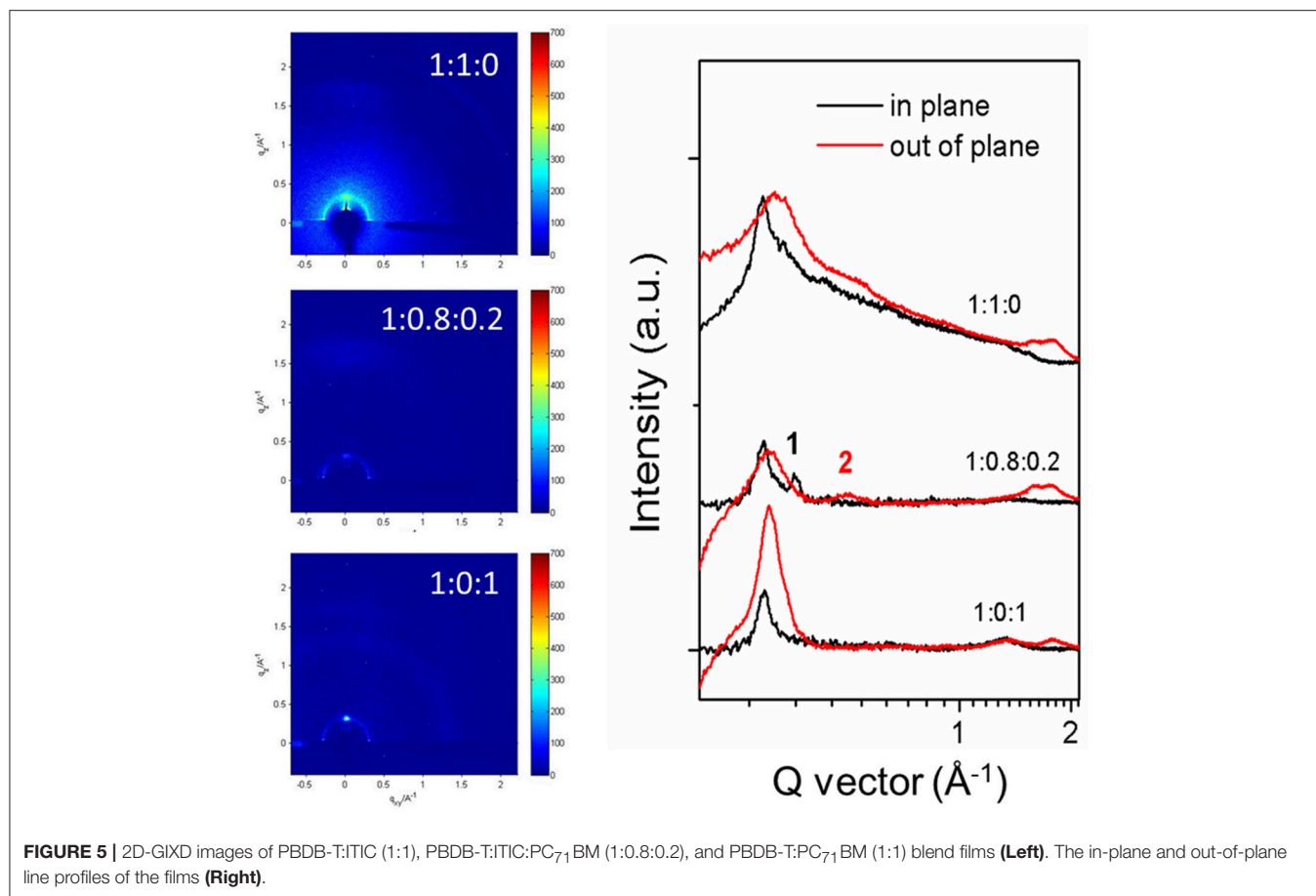
FIGURE 4 | (A) $J_{ph} - V_{eff}$ curves and **(B)** J_{SC} dependence on the illuminated light intensity of PSCs based on PBDB-T:ITIC (1:1), PBDB-T:ITIC:PC$_{71}$BM (1:0.8:0.2), and PBDB-T:PC$_{71}$BM (1:1) blend films, respectively.

(1:1), PBDB-T:ITIC:PC$_{71}$BM (1:0.8:0.2), and PBDB-T:PC$_{71}$BM (1:1) blends. The device based on ternary PBDB-T:ITIC:PC$_{71}$BM (1:0.8:0.2) blend demonstrates the highest saturation current, indicating its highest charge-generation capability. Charge dissociation probability P(E,T) is defined as J_{ph}/J_{sat}. When a high bias is applied, the charge recombination is suppressed and most of photo-generated charges are extracted, leading to P(E,T) close to100%. It is calculated that the P(E,T) values under short-circuit condition ($V_{appl} = 0$ V) are 90.6, 91.9, and 94.9%, respectively, for the PSCs based on the PBDB-T:ITIC (1:1), PBDB-T:ITIC:PC$_{71}$BM (1:0.8:0.2), and PBDB-T:PC$_{71}$BM (1:1) blends. The PBDB-T:PC$_{71}$BM (1:1) device shows the best charge-extraction capability, whereas the charge-extraction ability is a little poor for the PBDB-T:ITIC (1:1) device. The ternary PBDB-T:ITIC:PC$_{71}$BM (1:0.8:0.2) shows improved exciton dissociation and charge extraction compared to the PBDB-T:ITIC (1:1) device. The charge recombination status in these devices is also investigated via the dependence of J_{SC} on the incident light intensity as shown in **Figure 4B**. J_{SC} is dependent on the incident light intensity with $J_{SC} \propto I^\alpha$, in which exponential factor

α would be close to unity without bimolecular recombination (Gao et al., 2016; Xu et al., 2017, 2018). The PBDB-T:PC$_{71}$BM (1:1) device has the highest α value of 0.964, whereas α value of the PBDB-T:ITIC (1:1) device is merely 0.935 implying severe bimolecular recombination within the film. Such kind of bimolecular recombination in the PBDB-T:ITIC (1:1) device is to some extent suppressed with α value of 0.955 in ternary PBDB-T:ITIC:PC$_{71}$BM (1:0.8:0.2) device.

As discussed above, with the introduction of PC$_{71}$BM into the PBDB-T:ITIC blend, the resultant ternary PSCs demonstrate an enhanced exciton-dissociating and charge-extracting property, leading to improved PCE compared to the PBDB-T:ITIC PSCs. The detailed mechanism accounting for the enhancement is further investigated. The electron and hole transport properties of the various blend films were firstly measured via space-charge limited current (SCLC) method (Bin et al., 2016). The J-V curves of the devices were plotted as in Figure S1 and the calculated electron and hole mobility are listed in Table S2. The PBDB-T:PC$_{71}$BM (1:1) blend film shows relatively high electron and hole mobility of 8.45×10^{-4} and 5.30×10^{-4} cm^{2}V^{-1}s^{-1}, respectively. However, the electron and hole mobility of the PBDB-T:ITIC (1:1) film is 3.05×10^{-4} and 2.70×10^{-4} cm^{2}V^{-1}s^{-1}. After incorporating PC$_{71}$BM, the electron and hole mobility of the resultant PBDB-T:ITIC:PC$_{71}$BM (1:0.8:0.2) film is increased to 4.55×10^{-4} and 3.37×10^{-4} cm^{2}V^{-1}s^{-1}. As it is known, the high and balanced charge transport may help to efficient charge extraction and hence low charge recombination. This is in agreement with the recombination status in these PSCs. It is speculated that the incorporation of PC$_{71}$BM improves the PBDB-T and ITIC interpenetrating networks and thus the photovoltaic performance.

The morphology of the PBDB-T:ITIC (1:1), PBDB-T:ITIC:PC$_{71}$BM (1:0.8:0.2), and PBDB-T:PC$_{71}$BM (1:1) blend films are investigated and their AFM and TEM images are shown in Figures S2, S3. All the blend films are smooth with a root mean square (RMS) roughness of <2 nm. However, the morphology of the ternary blend is not changed obviously compared to the PBDB-T:ITIC (1:1) blend film. The structural information of the blended films are further investigated by grazing incidence X-ray diffraction (GIXD). The 2D-GIXD images of the pure PBDB-T and ITIC films are plotted in Figure S4. The pure PBDB-T film shows dominant peak at $q_{xy} = 0.29$ Å^{-1} in the in-plane direction, attributing to its strong (100) diffraction. The pure ITIC film demonstrates two featured peaks at $q_z = 0.26$ Å^{-1} and $q_z = 0.53$ Å^{-1} in out-of-plane direction and one peak in in-plane direction at $q_{xy} = 0.36$ Å^{-1}. 2D-GIXD patterns and line-cut profiles of the PBDB-T:ITIC (1:1), PBDB-T:ITIC:PC$_{71}$BM (1:0.8:0.2) and PBDB-T:PC$_{71}$BM (1:1) films are shown in **Figure 5**. The diffractions originated from PBDB-T aggregation is observed both in PBDB-T:ITIC (1:1) and PBDB-T:PC$_{71}$BM (1:1) films in contrast to the pure PBDB-T film. However, the diffraction signal originated from the ITIC component is not obviously presented in PBDB-T:ITIC blend film, implying its poor aggregation. In the PBDB-T:ITIC:PC$_{71}$BM (1:0.8:0.2) blend film, the diffraction signal from PBDB-T is still presented but weakened. More importantly, two additional peaks marked 1 and 2 are presented in the ternary blend film compared to the PBDB-T:ITIC (1:1)

FIGURE 5 | 2D-GIXD images of PBDB-T:ITIC (1:1), PBDB-T:ITIC:PC$_{71}$BM (1:0.8:0.2), and PBDB-T:PC$_{71}$BM (1:1) blend films **(Left)**. The in-plane and out-of-plane line profiles of the films **(Right)**.
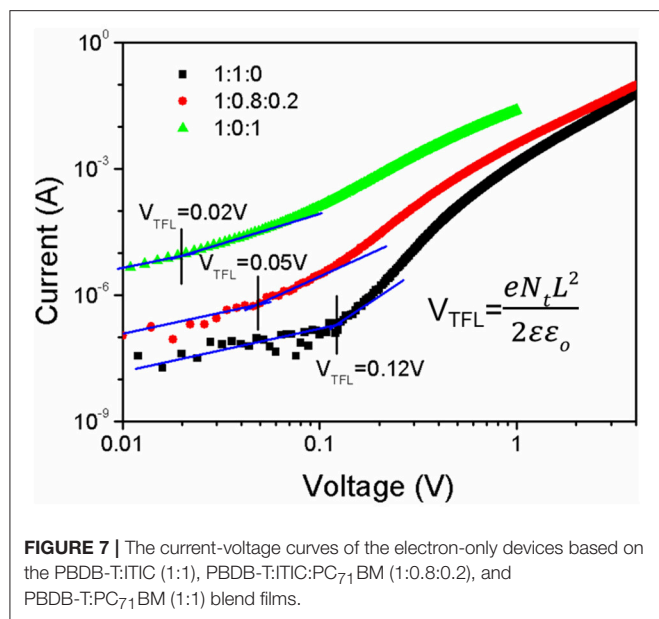
counterpart, which corresponds to the featured diffraction from ITIC in the in-plane and out-of-plane directions. Bo et al. observed similar phenomenon in their work (Lu et al., 2016). This indicates that the ITIC aggregation is enhanced in the PBDB-T:ITIC:PC$_{71}$BM (1:0.8:0.2) blend film though the ITIC content is decreased. In other words, the small amount of PC$_{71}$BM may serve as "lubricant" to favor ITIC molecules to aggregate out of the polymer PBDB-T matrix.

The prerequisite to get such a conclusion is that the compatibility between PBDB-T and PC$_{71}$BM should be better than that between PBDB-T and ITIC. The electron mobility of the PBDB-T:ITIC (1:x) and PBDB-T:PC$_{71}$BM (1:x) blend films are measured and its dependence on the acceptor ratio is plotted in **Figure 6**. It is supposed that the acceptor phase forms continuous tunnels when the electron mobility of the blend films exceeds 10^{-5} cm^{2}V^{-1}s^{-1}. Both the as-prepared film deposited in CB solution and the annealed film deposited in CB:DIO (0.5%, v/v) solution are tested. The results show that the continuous electron-transport tunnels is formed in the PBDB-T:ITIC film with the ITIC/PBDB-T ratio <20%. The DIO additive and thermal annealing donot change the electron transport remarkably. For the as-prepared PBDB-T:PC$_{71}$BM film, the critical PC$_{71}$BM content is increased to 25%. The DIO additive and thermal annealing lowers the critical PC$_{71}$BM content. This indicates that the PBDB-T is inclined to intermix

FIGURE 6 | The measured electron mobility in the PBDB-T:ITIC (1:x) and PBDB-T:PC$_{71}$BM (1:x) films.
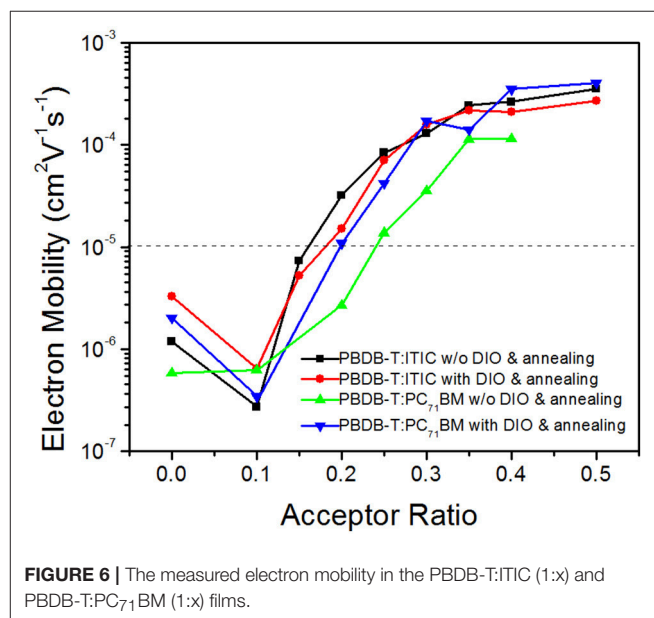
with PC$_{71}$BM better than with ITIC. In the ternary PBDB-T:ITIC:PC$_{71}$BM (1:0.8:0.2) blend film, the small amount of PC$_{71}$BM may mix with PBDB-T and does not form networks.

FIGURE 7 | The current-voltage curves of the electron-only devices based on the PBDB-T:ITIC (1:1), PBDB-T:ITIC:PC$_{71}$BM (1:0.8:0.2), and PBDB-T:PC$_{71}$BM (1:1) blend films.

Moreover, the existence of PC$_{71}$BM favors ITIC aggregating to form electron-transporting networks. This is confirmed by the increased electron mobility and the XRD results compared to the PBDB-T:ITIC (1:1) film.

The electron trap-state density in these blend films is further investigated. From the I–V curves of the electron-only devices based on the PBDB-T:ITIC (1:1), PBDB-T:ITIC:PC$_{71}$BM (1:0.8:0.2) and PBDB-T:PC$_{71}$BM (1:1) blend shown in **Figure 7**, the electron trap density N is calculated by the equation as below (Yang et al., 2016):

$$V_{TFL} = \frac{eNL^2}{2\varepsilon_0\varepsilon_r} \qquad (1)$$

where V$_{TFL}$ is the trap-filled limit voltage, e is the elementary charge of electron, L is the thickness of film, ϵ_0 is the vacuum permittivity, and ϵ_r is the relative dielectric constant (ϵ_r = 3). The V$_{TFL}$ of three devices is 0.12, 0.05, and 0.02 V. The calculated deep trap density is 3.3 × 10^{15}, 1.5 × 10^{15}, and 7.3 × 10^{14} cm^{-3}, respectively. It confirms that the incorporation of PC$_{71}$BM is helpful for ITIC molecules to move out of PBDB-T phases and thus the density of electron traps is reduced. The increased electron mobility and the decreased electron traps are

helpful to enhance the photovoltaic performance of the PBDB-T:ITIC:PC$_{71}$BM (1:0.8:0.2).

CONCLUSION

In summary, the ternary PSCs based on PBDB-T:ITIC:PC$_{71}$BM (1:0.8:0.2) blend were fabricated and its PCE was increased to 10.2% compared to 9.2% for the PBDB-T:ITIC (1:1) devices. The mechanism accounting for the enhanced photovoltaic performance is discussed in detail. It is found that the PC$_{71}$BM tends to intermix with the PBDB-T donor compared to the ITIC counterpart. A small amount of PC$_{71}$BM in the ternary blend is helpful for ITIC to aggregate and form efficient electron-transport pathways. The electron mobility is increased and the density of electron traps is decreased in the ternary PBDB-T:ITIC:PC$_{71}$BM (1:0.8:0.2) blend in comparison with the PBDB-T:ITIC blend. Finally, the suppressed bimolecular recombination and enhanced charge collection lead to a high PCE for the ternary solar cells.

AUTHOR CONTRIBUTIONS

BW and CY conceived and designed the experiments. BW performed the experiments. RZ performed 2D-GIXD measurements. QY performed the absorption and PL experiments. BW and YF analyzed data. BW wrote the manuscript. All authors discussed and commented on the paper.

ACKNOWLEDGMENTS

SUPPLEMENTARY MATERIAL

The Supplementary Material for this article can be found online at: https://www.frontiersin.org/articles/10.3389/fchem.2018.00198/full#supplementary-material

REFERENCES

Bin, H., Zhang, Z. G., Gao, L., Chen, S., Zhong, L., Xue, L., et al. (2016). Non-fullerene polymer solar cells based on alkylthio and fluorine substituted 2D-conjugated polymers reach 9.5% efficiency. *J. Am. Chem. Soc.* 138, 4657–4664. doi: 10.1021/jacs.6b01744

Cao, Q., Xiong, W., Chen, H., Cai, G., Wang, G., Zheng, L., et al. (2017). Design, synthesis, and structural characterization of the first dithienocyclopentacarbazole-based ntype organic semiconductor and its application in non-fullerene polymer solar cells. *J. Mater. Chem. A* 5, 7451–7461. doi: 10.1039/C7TA01143A

Cheng, P., Li, Y., and Zhan, X. (2014). Efficient ternary blend polymer solar cells with indene-C60 bisadduct as an electron-cascadeacceptor. *Energy Environ. Sci.* 7, 2005–2011. doi: 10.1039/c3ee44202k

Dai, S., Li, T., Wang, W., Xiao, Y., Lau, T. K., Li, Z., et al. (2018). Enhancing the performance of polymer solar cells via core engineering of nir-absorbing electron acceptors. *Adv. Mater.* 30:e1706571. doi: 10.1002/adma.201706571

Fan, Q., Su, W., Guo, X., Wang, Y., Chen, J., Ye, C., et al. (2017). Side-chain engineering for efficient non-fullerene polymer solar cells based on a wide-bandgap polymer donor. *J. Mater. Chem. A* 5, 9204–9209. doi: 10.1039/C7TA02075A

Gao, L., Zhang, Z. G., Bin, H., Xue, L., Yang, Y., Wang, C., et al. (2016). High-efficiency nonfullerene polymer solar cells with medium bandgap polymer donor and narrow bandgap organic semiconductor acceptor. *Adv. Mater.* 28, 8288–8295. doi: 10.1002/adma.201601595

Gasparini, N., Jiao, X., Heumueller, T., Baran, D., Matt, G., Fladischer, S., et al. (2016). Designing ternary blend bulk heterojunction solar cells with reduced carrier recombination and a fill factor of 77%. *Nat. Energy* 1:16118. doi: 10.1038/nenergy.2016.118

Holliday, S., Ashraf, R. S., Wadsworth, A., Baran, D., Yousaf, S. A., Nielsen, C. B., et al. (2016). High-efficiency and air-stable P3HT-based polymer solar cells with a new non-fullerene acceptor. *Nat. Commun.* 7:11585. doi: 10.1038/ncomms11585

Jiang, W., Yu, R., Liu, Z., Peng, R., Mi, D., Hong, L., et al. (2018). Ternary nonfullerene polymer solar cells with 12.16% efficiency by introducing one acceptor with cascading energy level and complementary absorption. *Adv. Mater.* 30:1703005. doi: 10.1002/adma.201703005

Li, S., Ye, L., Zhao, W., Zhang, S., Ade, H., and Hou, J. (2017). Signifcant influence of the methoxyl substitution position on optoelectronic properties and molecular packing of small-molecule electron acceptors for photovoltaic cells. *Adv. Energy Mater.* 7:1700183. doi: 10.1002/aenm.201700183

Li, S., Ye, L., Zhao, W., Zhang, S., Mukherjee, S., Ade, H., et al. (2016). Energy-level modulation of small-molecule electron acceptors to achieve over 12% effciency in polymer solar cells. *Adv. Mater.* 28, 9423–9429. doi: 10.1002/adma.201602776

Li, S., Zhan, L., Liu, F., Ren, J., Shi, M., Li, C. Z., et al. (2018). An unfused-core-based nonfullerene acceptor enables high-efficiency organic solar cells with excellent morphological stability at high temperatures. *Adv. Mater.* 30:1705208. doi: 10.1002/adma.201705208

Lin, Y., Wang, J., Zhang, Z. G., Bai, H., Li, Y., Zhu, D., et al. (2015). An electron acceptor challenging fullerenes for efficient polymer solar cells. *Adv. Mater.* 27, 1170–1174. doi: 10.1002/adma.201404317

Lu, H., Zhang, J., Chen, J., Liu, Q., Gong, X., Feng, S., et al. (2016). Ternary-blend polymer solar cells combining fullerene and nonfullerene acceptors to synergistically boost the photovoltaic performance. *Adv. Mater.* 28, 9559–9566. doi: 10.1002/adma.201603588

Lu, L., Kelly, M., You, W., and Yu, L. (2015). Status and prospects for ternary organic photovoltaics. *Nat. Photonics* 9, 491–500. doi: 10.1038/nphoton.2015.128

Qiu, N., Zhang, H., Wan, X., Li, C., Ke, X., Feng, H., et al. (2017). A new nonfullerene electron acceptor with a ladder type backbone for high-performance organic solar cells. *Adv. Mater.* 29:1604964. doi: 10.1002/adma.201604964

Wang, J., Peng, J., Liu, X., and Liang, Z. (2017). Efficient and stable ternary organic solar cells based on two planar nonfullerene acceptors with tunable crystallinity and phase miscibility. *ACS Appl. Mater. Interfaces* 9, 20704–20710. doi: 10.1021/acsami.7b03757

Wang, Z., Zhu, X., Zhang, J., Lu, K., Fang, J., Zhang, Y., et al. (2018). From alloy-like to cascade blended structure: designing high-performance all small molecule ternary solar cells. *J. Am. Chem. Soc.* 140, 1549–1556. doi: 10.1021/jacs.7b13054

Xiao, Z., Jia, X., Li, D., Wang, S., Geng, X., Liu, F., et al. (2017). 26 mA cm−2 Jsc from organic solar cells with a low-bandgap nonfullerene acceptor. *Sci. Bull.* 62, 1494–1497. doi: 10.1016/j.scib.2017.10.017

Xu, S., Wang, X., Feng, L., He, Z., Peng, H., Cimrová, V., et al. (2018). Optimizing the conjugated side chains of quinoxaline based polymers for nonfullerene solar cells with 10.5% efficiency. *J. Mater. Chem. A* 6, 3074–3083. doi: 10.1039/C7TA10262C

Xu, X., Bi, Z., Ma, W., Wang, Z., Choy, W. C. H., Wu, W., et al. (2017). Highly efficient ternary-blend polymer solar cells enabled by a nonfullerene acceptor and two polymer donors with a broad composition tolerance. *Adv. Mater.* 29:1704271. doi: 10.1002/adma.201704271

Yang, D., Yang, R., Ren, X., Zhu, X., Yang, Z., Li, C., et al. (2016). Hysteresis-suppressed high-efficiency flexible perovskite solar cells using solid-state ionic-liquids for effective electron transport. *Adv. Mater.* 28, 5206–5213. doi: 10.1002/adma.201600446

Yu, R., Zhang, S., Yao, H., Guo, B., Li, S., Zhang, H., et al. (2017). Two well-miscible acceptors work as one for efficient fullerene-free organic solar cells. *Adv. Mater.* 29:1700437. doi: 10.1002/adma.201700437

Yuan, J., Guo, W., Xia, Y., Ford, M. J., Jin, F., Liu, D., et al. (2017). Comparing the device physics, dynamics and morphology of polymer solar cells employing conventional PCBM and non-fullerene polymer acceptor N2200. *Nano Energy* 35, 251–262. doi: 10.1016/j.nanoen.2017.03.050

Zhang, G., Zhang, K., Yin, Q., Jiang, X. F., Wang, Z., Xin, J., et al. (2017). High-performance ternary organic solar cell enabled by a thick active layer containing a liquid crystalline small molecule donor. *J. Am. Chem. Soc.* 139, 2387–2395. doi: 10.1021/jacs.6b11991

Zhang, J., Zhao, Y., Fang, J., Yuan, L., Xia, B., Wang, G., et al. (2017). Enhancing performance of large-area organic solar cells with thick film via ternary strategy. *Small* 13:1700388. doi: 10.1002/smll.201700388

Zhang, Z., Qi, B., Jin, Z., Chi, D., Qi, Z., Li, Y., et al. (2014). Perylene diimides: a thickness-insensitive cathode interlayer for high performance polymer solar cells. *Energy Environ. Sci.* 7, 1966–1973. doi: 10.1039/c4ee00022f

Zhao, W., Li, S., Zhang, S., Liu, X., and Hou, J. (2017). Ternary polymer solar cells based on two acceptors and one donor for achieving 12.2% effciency. *Adv. Mater.* 29:1604059. doi: 10.1002/adma.201604059